1-2013

A Thermodynamic Analysis of an Intense North American Arctic Air Mass

Jessica K. Turner
McGill University

John Gyakum
McGill University

Shawn M. Milrad
McGill University, milrads@erau.edu

A Thermodynamic Analysis of an Intense North American Arctic Air Mass

JESSICA K. TURNER, JOHN GYAKUM, AND SHAWN M. MILRAD

Department of Atmospheric and Oceanic Sciences, McGill University, Montreal, Quebec, Canada

(Manuscript received and in final form 15 June 2012)

ABSTRACT

Northwestern Canada is a genesis region of arctic air masses often considered to be formed primarily through radiative processes. However, the details of their life cycle are poorly understood. This paper examines the formation, maintenance, and dissipation of an intense and long-lived arctic air mass, using a thermodynamic budget analysis.

The airmass formation is characterized by a deep-layer, multistage process that begins with snow falling into a nascent air mass. Radiative cooling from cloud tops begins the process. After the snow abates and clear skies are observed, the surface temperature drops rapidly, aided by the high emissivity of fresh snow cover, falling 17°C in two days, creating an intense but shallow temperature inversion. Once the surface temperature falls below the frost point, ice crystals form. Afterward, although the surface temperature remains constant, the height of the inversion rises, as radiative cooling at the top of the ice fog layer decreases temperatures.

During the maintenance phase, a cold-air damming structure is present with an anticyclone in the lee of the Canadian Rockies, low pressure in the Gulf of Alaska, and an intense baroclinic zone parallel to the mountains, separating warmer maritime air from colder continental air. The air mass persists for 12 days, undergoing several cycles of deep-layer weakening and intensification.

1. Introduction

Northwestern Canada is an important formation and development region for the winter weather phenomenon known as arctic air masses, also called continental polar air masses. Turner and Gyakum (2011) studied the composite characteristics of their creation and intensification. The air masses formed at an average rate of 1.5 yr^{-1} over the period 1948–2008, with an average surface temperature at 10 stations in northwest Canada during the events of −39.6°C: 1.65 standard deviations colder than the climatological daily winter [December–February (DJF)] temperature at these stations. Contrary to the classic view of their structure as a shallow temperature inversion created through surface radiation alone, these air masses typically develop through a deep layer in multiple stages, with in situ intensification and associated cold-air damming. Surface radiation has a role, but the diabatic processes of ice crystal radiation and sublimation were also found to be important.

Corresponding author address: Shawn M. Milrad, 805 Sherbooke St.West, Montreal, QC H3A 2K6, Canada.
E-mail: shawn.milrad@gmail.com

DOI: 10.1175/MWR-D-12-00176.1

The first model of arctic airmass formation was made by Wexler (1936, 1937) by assuming radiative equilibrium between a snow-covered surface and an isothermal atmosphere. The surface radiates as a blackbody in the model, while the atmosphere in contact with the surface loses heat to it. Since the surface loses heat more quickly than the atmosphere, it continues to cool, creating a shallow temperature inversion. However, this model was known to underestimate the rate and depth of cooling compared to observations. It took an unrealistic 26 days for the surface temperature to drop from 0° to −36°C and for the height of the inversion to reach 4 km.

Wexler model's underestimation arises from an absence of ice crystals. Gotaas and Benson (1965) first proposed their importance in arctic airmass formation. Ice crystals act as a heat sink for the atmosphere, absorbing then radiating heat, cooling the atmospheric layer in which they are embedded. This effect was quantified by Curry (1983) in a one-dimensional radiative transfer model including subsidence, microphysics, and turbulent mixing. Curry (1983) was able to produce the same amount of cooling as Wexler (1936, 1937) in 14 days instead of 26, noting that the cooling rate was sensitive to the amount of condensate in the air mass. Increasing the

TABLE 1. The 10 stations used in the study and their latitude, longitude, altitude, and climatological mean daylight amount during the event, 2–13 Feb, listed from most northern to most southern. Boldface station names indicate rawinsonde stations.

Station	Lat (°N)	Lon (°W)	Altitude (m)	Mean daylight (h)
Sachs Harbour, Northwest Territories	72.0	125.3	86	4.5
Inuvik, Northwest Territories	68.3	133.5	68	6.3
Kugluktuk, Nunavut	67.8	115.1	23	6.5
Norman Wells, Northwest Territories	65.3	126.8	74	7.2
Yellowknife, Northwest Territories	62.5	114.4	206	7.9
Fort Simpson, Northwest Territories	61.8	121.2	169	8.0
Fort Smith, Northwest Territories	60.0	112.0	205	8.3
Fort Nelson, British Columbia	58.8	122.6	382	8.5
Fort McMurray, Alberta	56.7	111.2	369	8.8
Grande Prairie, Alberta	55.2	118.9	669	9.0

condensate in a layer increases radiative cooling in that layer, while warming the surface. More recently, Emanuel (2008) used a single-column, radiative-convective model, beginning with a tropical sounding, to simulate the formation of arctic air. Emanuel (2008) showed that the rate and depth of the cooling were sensitive to the amount of water vapor, condensate, and clouds. When clouds were allowed to form, air in contact with the cloud top cooled through radiation, while warming the lower layers through radiation and latent heat release.

High-latitude northwestern North America is observed to be warming, especially during the winter season (Jones and Moberg 2003; Serreze and Francis 2006; Serreze et al. 2000; Shabbar and Bonsal 2003). Arctic cloud processes are important in the energy budget and climate of the region (Sorteberg et al. 2007; Vavrus et al. 2008) and they are poorly parameterized in reanalysis datasets and other models (Intrieri and Shupe 2004; Intrieri et al. 2002; Liu et al. 2005; Town et al. 2005; Walsh et al. 2009). To better understand the processes involved in the creation of these events, this paper examines the dynamics and thermodynamics associated with the formation and maintenance of an intense, but characteristic arctic air mass, selected from 93 events in Turner and Gyakum (2011). The event chosen, spanning 2–13 February 1979, is notable for its large vertical depth of cooling and areal coverage. Its duration is in the 98th percentile of event length: it lasted 17 days compared to the mean of 5 days. The minimum surface temperature observed during the event was −48.1°C, at Norman Wells, Northwest Territories, on 8 February, more than three standard deviations below the climatological value of −28.5°C, over the period of 1944–2010, for that station and month.

2. Data and methodology

a. Data and event choice

A total of 10 stations in northwestern Canada with good-quality long-term daily temperatures were chosen. This dataset, provided by the Meteorological Service of Canada, has been corrected for nonclimatic inhomogeneities from sources such as changes in instrumentation or location (Vincent et al. 2002). There also exist continuous hourly surface observations from the Environment Canada National Climate Data and Information Archive at all stations. Twice daily (0000 and 1200 UTC) rawinsonde soundings are available at several of the stations.

Table 1 lists the name, latitude, longitude, altitude, and average length of day during the event period at the 10 stations. During the winter months these stations have extremely short days, solar insolation is low, and there is a near absence of the diurnal cycle. The geographical location of the stations, with orography, is shown in Fig. 1. The stations have generally low elevation, with the exception of Grande Prairie at 669 m. The orography of the region has profound consequences on the air masses that form there. The Rocky Mountains impede most eastward atmospheric flow below 800 hPa (Lackmann et al. 1998) and separate the maritime air masses of the northeast Pacific Ocean from the continental interior. The altitude gradient is substantial and the stations used in this study, located in the lee of the mountains, are nearly at sea level. A few outlets for continental air exist: there are networks of glaciers in the mountains and gap flow is possible. Another outlet from the interior is through the Alaskan highlands and lowlands, a channel of lower elevation terrain lying between the Alaskan and Brooks Ranges, through which cold air can drain into the Bering Sea.

The National Centers for Environmental Prediction (NCEP) North American Regional Reanalysis (NARR; Mesinger et al. 2006) is used for upper-air heights, temperature, mixing ratio, and wind field values. The NARR has a spatial resolution of 32 km at 40°N and a temporal resolution of 3 h. The high spatial resolution is particularly valuable in the intermountain region as the topography responsible for gap flow and other small-scale

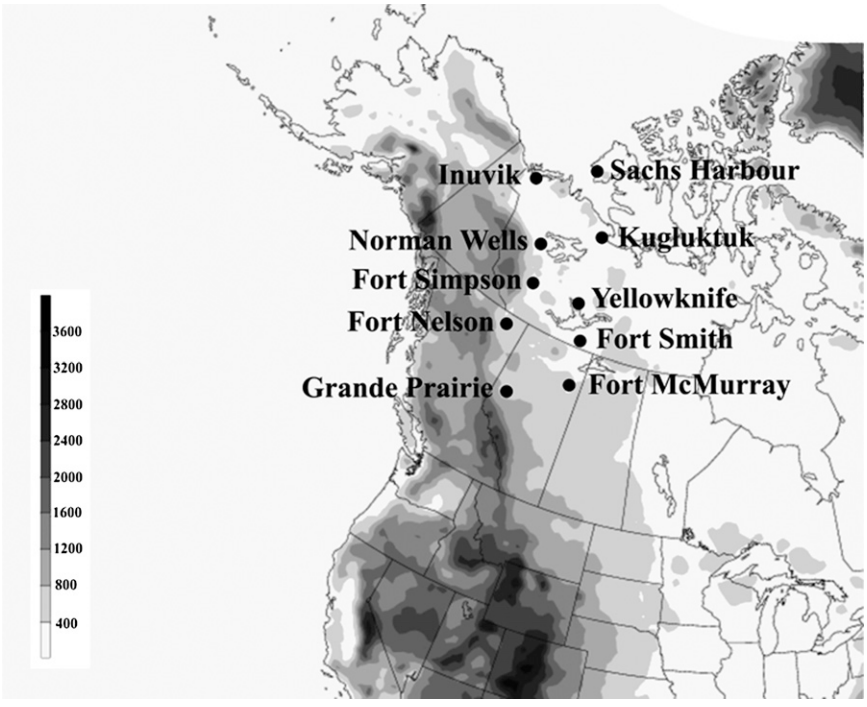

FIG. 1. A total of 10 stations in and around the Mackenzie River basin with long-term hourly observations. Inuvik, Norman Wells, and Fort McMurray launch twice-daily rawinsonde at 0000 and 1200 UTC. Elevation shading contours are in m.

features can be captured. Owing to the importance of microphysics acting on a subgrid scale, the NARR reanalysis may not accurately capture all processes during the event. We compared NARR soundings to actual soundings (not shown) and found that while the upper atmosphere was well represented, the depth and intensity of near-surface inversions were not well captured. At Norman Wells, the RMSE of the NARR temperature over the course of the event 27 January–13 February 1979 compared to the soundings is 7.4°C at 1000 hPa, 2.1°C at 850 hPa, and 0.9°C at 500 hPa. The NARR temperature is warm biased al low levels during the event, being 21% warmer than the soundings at 1000 hPa and 6% warmer at 850 hPa, but is unbiased at 500 hPa. The RMSE of NARR dewpoint is slightly lower at 1000 hPa (5.1°C), but slightly higher 3.7°C at 850 hPa and 1.9°C at 500 hPa. Walsh et al. (2009) showed that when the NARR correctly captured the cloud fraction at Barrow, Alaska, the radiative fluxes were well simulated. However, it tended to overestimate wintertime cloud fraction.

Turner and Gyakum (2011) defined arctic airmass events as 3 or more consecutive days of surface minimum temperature anomaly that is at least one standard deviation colder than the 30-yr running-mean monthly climatology for that station and month. This criterion must be satisfied in at least 5 of the 10 stations. The purpose of this event definition was to select synoptic-scale events from throughout the 1948–2008 period, rather than clustered at the beginning of the period—as would occur because of the surface warming trend. This definition also selects events throughout the winter (DJF) rather than only during January, the month of maximum variability.

Turner and Gyakum (2011) found that these arctic air masses were, contrary to the classic conception, deep-layer events with cooling extending up to 500 hPa, rather than being solely shallow, surface radiation–driven events. They were found to form in multistages, beginning with snow falling into a drier surface layer, increasing low-level moisture and cooling the upper atmosphere through radiation from cloud tops. After the atmosphere cleared, upwelling longwave radiation decreased surface temperatures rapidly until ice crystals and ice fog formed. Finally, the ice fog halted further cooling at the surface but increased radiation cooling at the top of the fog layer, creating more ice crystals at the boundary and thus increasing both the height of the fog layer and the temperature inversion.

The 1979 event discussed in this paper was selected for its duration and intensity from a larger set of 93 arctic airmass events that met the selection criterion. Figure 2

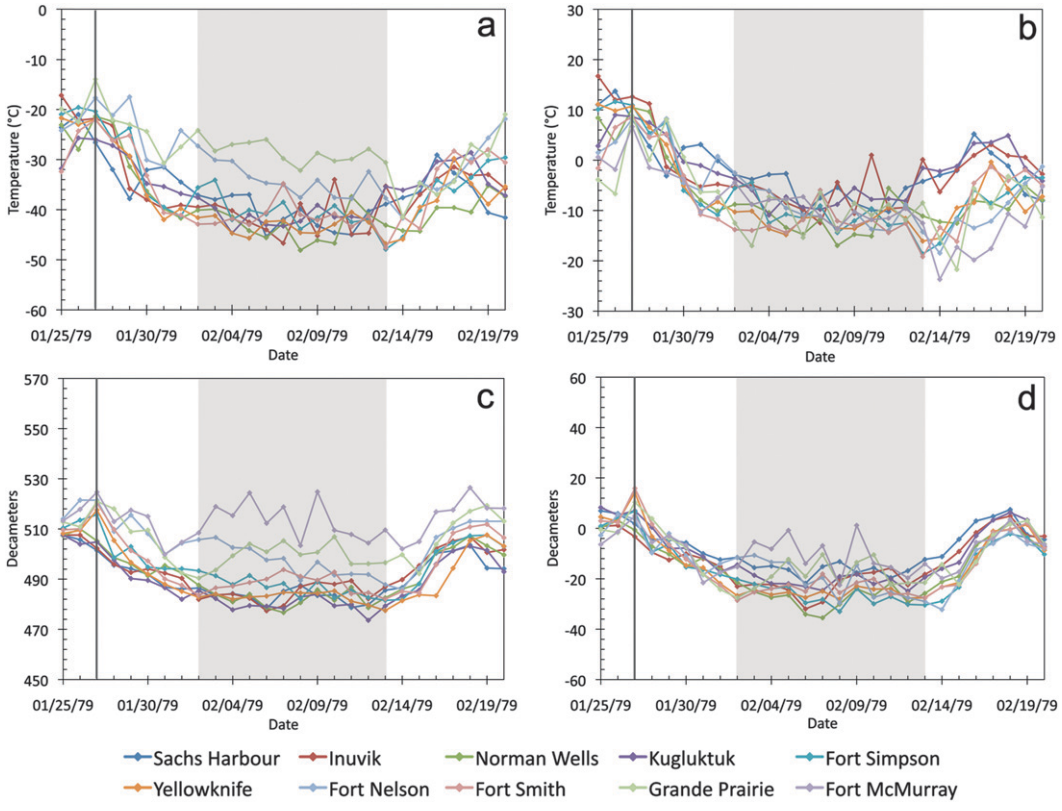

FIG. 2. Daily (a) minimum surface temperature, (b) minimum surface temperature anomalies, (c) 1000–500-hPa thicknesses at 1200 UTC and (d) 1000–500-hPa thickness anomalies for 10 stations. The vertical solid line indicates the start of the formation period. The maintenance period is shaded.

shows the time series of daily surface minimum temperature, temperature anomaly, 1000–500-hPa thickness, and thickness anomaly relative to the period 1979–2008. The temperatures and thicknesses begin falling several days before the event definition criteria are met. Based on Fig. 2, a formation period was defined beginning with the first temperature falls at Norman Wells and ending at the start of the event itself. The formation period is 27 January–1 February 1979. The event, defined by the Turner and Gyakum (2011) criteria and hereafter called the maintenance period, occurs from 2–12 February. During this time, the surface temperatures and thicknesses are more constant than during the formation, although some oscillation between warmer and colder days occurs. The air mass begins to leave the region on 13 February, causing rapid thickness increases (Fig. 2c).

b. Methodology

A thermodynamic budget was calculated from the NARR at the 1000-, 925-, 850-, 700-, 600-, and 500-hPa levels using the thermodynamic equation on a constant pressure surface:

$$\frac{\partial T}{\partial t} = -\mathbf{v}\cdot\nabla_H T + \omega\left(\frac{\alpha}{C_p} - \frac{\partial T}{\partial p}\right) + \frac{1}{C_p}\frac{dQ}{dt}, \quad (1)$$

A B C D

where T is the temperature (K), t is time (s), $\mathbf{v}$ is the horizontal wind field (m s^{-1}), ∇_H is the horizontal gradient, ω is the vertical velocity (hPa s^{-1}), α is the specific volume RT/p where R is the dry gas constant (287 J kg^{-1} K^{-1}), C_p is the specific heat capacity at constant pressure (1005 J kg^{-1} K^{-1}), p is the pressure (hPa), and Q is diabatic heating (J kg^{-1}; Rogers and Yau 1989). The time change in temperature at an individual station (term A) is equal to horizontal advection (term B) plus the vertical term (adiabatic expansion/compression and vertical advection, term C) and the diabatic heating term (term D). Diabatic heating includes sensible and latent heating, along with radiative processes.

To calculate the terms, finite differences were substituted for derivatives. The 3-hourly (the temporal resolution of the NARR) finite time differences of a term are the average of the instantaneous value at the period's two endpoints, multiplied by 3 h. The vertical term has finite differences in the vertical. The $\partial T/\partial p$ finite difference is

the difference in temperature between 1000–925, 1000–850, 925–700, 850–600, 700–500, and 600–400 hPa for the 1000-, 925-, 850-, 700-, 600-, and 500-hPa levels, respectively. The daily temperature change at a grid point (left-hand side) is the difference in temperature at 1200 UTC from one day to the next. The total daily value of horizontal advection and vertical terms (right-hand side) is the daily sum of eight 3-hourly periods. Finally, the diabatic term is the residual of term A minus terms B and C. Since we have seen that the NARR is warm biased at low levels during the event residual cooling is likely to be underestimated.

We assume that the atmosphere is unsaturated, which will introduce error in the calculation: surface observations of falling snow show that the atmosphere is saturated at some levels. Incorrectly assuming unsaturated ascent will make the magnitude of the adiabatic cooling in the vertical term too large with an equivalently large error of increased warming through latent heating existing in the residual term. At these temperatures the magnitude of the error will be small; for example, the difference between saturated and unsaturated ascent starting from −20°C at 850 hPa to 600 hPa is approximately 2°C.

The terms of the thermodynamic budget are interpolated to the 10 stations, using a bilinear interpolation scheme in GEMPAK, then vertically averaged using a weighted mean over lower (1000–850 hPa) and upper (850–500 hPa) layers. The weighted mean is calculated by

$$\bar{x} = \frac{\sum_{i-1}^{n} w_i x_i}{\sum_{i-1}^{n} w_i}, \tag{2}$$

where $\bar{x}$ is the weighted average, x_i is the NARR value at an individual station, and w_i is the weight at the ith measurement. The weights were chosen based on the depth (in hPa) between levels, with values of 0.25, 0.5, and 0.25 for the 1000-, 925-, and 850-hPa levels in the lower-layer calculation and 0.21, 0.36, 0.29, and 0.14 for the 850-, 700-, 600-, and 500-hPa levels in the upper-layer calculation. Standard errors for the weighted means are calculated by

$$Z = \sqrt{\frac{\sigma^2}{\sum_{i-1}^{n} w_i}}, \tag{3}$$

where σ^2 is the weighted variance:

$$\sigma^2 = \frac{\sum_{i-1}^{n} w_i (x_i - \bar{x})^2}{\sum_{i-1}^{n} w_i}. \tag{4}$$

3. Formation

a. Synoptic overview

During the formation period, an ocean–continent thickness contrast develops, strongest along the Alaskan and British Columbian coast, with colder air over the Canadian interior. Figure 3 shows the sea level pressure, 700-hPa winds and 1000–500-hPa thicknesses at 1200 UTC daily during the formation. The 700-hPa level has been found to be the level of maximum moisture transport into the Mackenzie River basin (Lackmann et al. 1998) and is mostly unobstructed by the mountains. From 27–28 January (Figs. 3a,b), the 1000–500-hPa thickness falls first over the frozen Arctic Ocean and the northern coast of the Northwest Territories (NWT). The Aleutian low, climatologically in the Gulf of Alaska, is shifted to the west. On 28 January (Fig. 3b), a tongue of 1032-hPa sea level pressure extends from Asia (not shown) into the Canadian northwest to east of the mountains.

From 29–31 January (Figs. 3c–e) the 1000–500-hPa thickness continues to fall across western Canada with a strengthening trough owing to cold-air advection from the Arctic Ocean over north-central Canada. On the last day of formation, 1 February (Fig. 3f), the coldest air, 470 dam, remains east of the Mackenzie River basin but very cold air is also present across western Canada. The 700-hPa flow in northwestern Canada is largely equivalent barotropic in the northwest with an intense temperature and sea level pressure gradient parallel to the coastal mountains. The anomaly fields were also calculated (not shown). The coldest 1000–500-hPa thickness anomaly, −28 dam, is centered over Great Slave Lake (bordering Yellowknife, Fig. 1). The greatest sea level pressure anomaly, 16 hPa, is a closed contour following the lee of the Mackenzie Mountains.

Weather observations inside the air mass are indicative of a multistage formation process. Table 2 lists the mean surface temperature and reported weather each day, as a percentage of total reports, partitioned into five northern and five southern stations. The northern stations are located more centrally in the western part of the developing air mass (Figs. 3a–f), while the southern stations are located along the western and southern edges. At the northern stations (Table 2) snow fell from 27–29 January, accompanied by moderate surface temperature falls. From 29–31 January the snow abated,

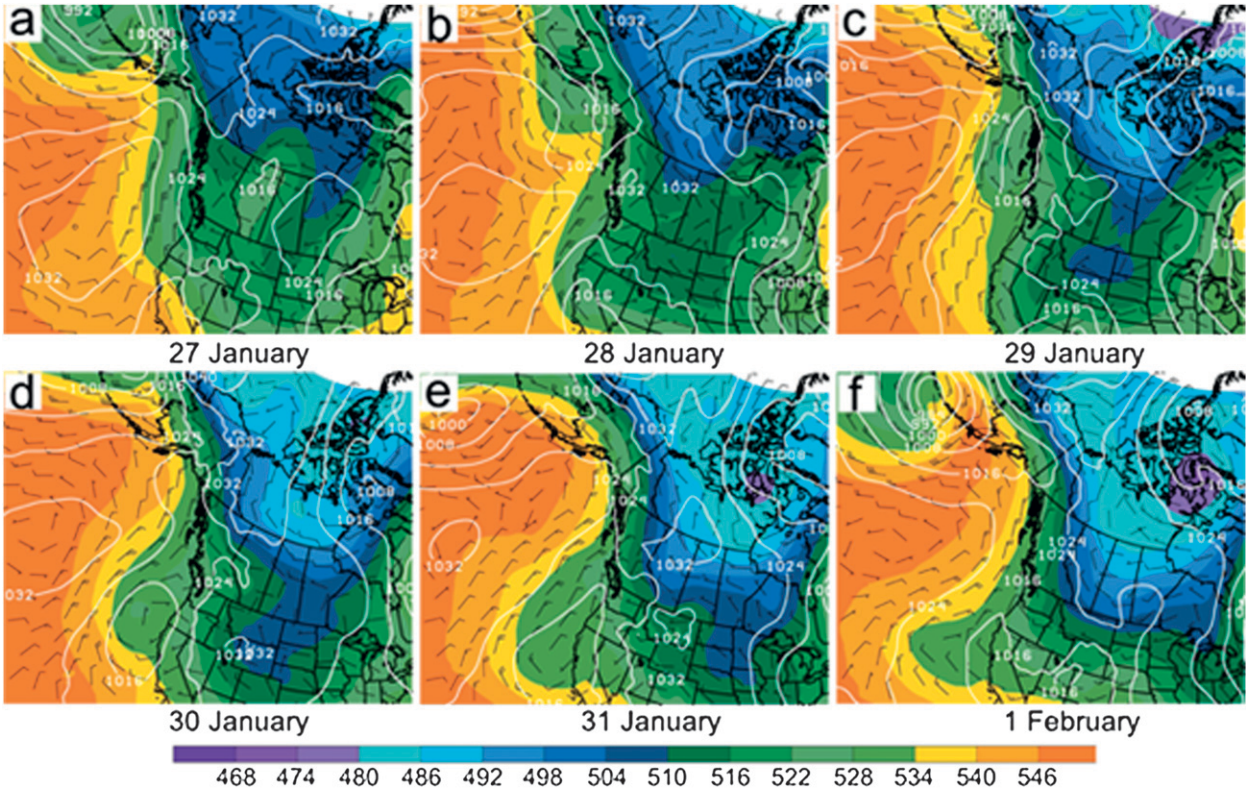

FIG. 3. Sea level pressure (contours, every 4 hPa), 700-hPa winds (barbs, m s^{-1}), and 1000–500-hPa thicknesses (shaded, every 6 dam) at 1200 UTC daily during the formation period.

clear skies were reported, and the average surface temperature dropped very rapidly, by 11°C over the two days. At the end of the formation period, 31 January–1 February, ice crystals and ice fog were reported. The importance of ice crystals to deep-layer cooling will be discussed further in section 4.

At the southern stations (Table 2), snow was reported less frequently on 27 January than at the northern stations and the weather reports alternate between snow and clear throughout the remainder of the formation period. An examination of the contribution of the individual stations showed that snow was more common at the higher-elevation stations, specifically Fort Nelson and Fort McMurray, whereas clear reports were most common at Fort Simpson. The average snow accumulation during the formation at the 10 stations is 2.3 cm, with the largest amount (6.6 cm) at Fort Nelson.

Daily soundings at 1200 UTC during the formation at Norman Wells—a station centrally located in the developing air mass—are shown in Fig. 4. On 27–28 January, the atmosphere is completely saturated from 925–700 hPa, indicating the presence of thick clouds. During this period, snow is reported at the surface of the northern stations (Table 2). In the sounding from 27–28 January (Fig. 4a) there is cooling at 700 hPa, most likely by cloud-top radiative cooling in the absence of cold advection (backing winds). A slight backing wind profile is first evident on 28 January in the 1000–700-hPa layer. On 29 January the base and top of the saturated layer rose, while the atmosphere became stable throughout most of its depth as the anticyclone formed.

On 30 January, clear skies and calm winds were reported at Norman Wells but the surface temperature had cooled dramatically—suggesting surface radiational cooling. The soundings show an intense temperature inversion at this time, much stronger than from 27–28 January. By 31 January the surface temperatures fell to their frost point: ice fog was reported (Table 2) at this time. Examining the surface observations (not shown), we find that snow stopped at 0800 UTC 29 January and ice fog formed at 0900 UTC 31 January. Over that period, the surface temperature fell from 17.6° to −37.5°C. For the remaining two formation days, the weather reports consisted primarily of ice crystals and ice fog (Table 2). The surface temperature fell less quickly; however, the height of the inversion rose on 31 January–1 February (Fig. 4). Modeling (Girard and Blanchet 2001) and observational studies (Wendler 1969) of

TABLE 2. Mean surface temperature and weather reports (as a percentage of total reports) at the northern stations (Sachs Harbour, Inuvik, Kugluktuk, Norman Wells, and Yellowknife) and southern stations (Fort Simpson, Fort Smith, Fort Nelson, Fort McMurray, and Grande Prairie) from 1200–1200 UTC daily. Most frequent observations on a given day are given in boldface.

	Surface temperature (°C)	Clear/mainly clear	Cloudy/mostly cloudy	Ice crystals/ice fog	Snow/blowing snow
			Northern stations		
27–28 Jan	−19.7	6	17	6	**71**
28–29 Jan	−22.6	19	21	13	**47**
29–30 Jan	−28.4	**39**	9	27	25
30–31 Jan	−33.6	**73**	0	24	3
31 Jan–1 Feb	−35.8	24	7	**61**	8
1–2 Feb	−35.7	18	0	**68**	15
			Southern stations		
27–28 Jan	−14.1	30	**38**	0	33
28–29 Jan	−17.8	**46**	37	1	17
29–30 Jan	−17.8	13	29	8	**50**
30–31 Jan	−24.9	**42**	13	16	29
31 Jan–1 Feb	−30.2	**36**	21	32	12
1–2 Feb	−28.8	12	16	35	**36**

North American arctic ice fogs have shown that they warm the surface through radiation.

Over the entire formation period, the greatest temperature decrease above the surface is at the 1000-hPa level, −15.1°C over six days, a rate comparable to that found by Curry (1983). The sounding also shows that rather than being restricted to the surface, there is a deep vertical extent to the cooling, with −13.9°C at 925 hPa, −8.7°C at 850 hPa, −9.0°C at 700 hPa, and −3.5°C at the 500-hPa level over the formation period.

b. The thermodynamic budget

The daily thermodynamic budget, layer-averaged using Eq. (2), over the 1000–850- and 850–500-hPa layers at the northern and southern stations is presented in Table 3. The values for the northern and southern stations were calculated by averaging the values derived from the bilinear interpolation described in section 2b. The 700-hPa wind direction in northwestern Canada was northwesterly during the formation (Figs. 3a–f). Therefore, the southern stations had larger values of cold-air advection owing to the production of cold air to the north. At all stations there were large values of cooling present in the lower and upper layers on most formation days. There was an easterly wind, and therefore upsloping, at low levels after 31 January at Norman Wells and at other stations along the mountains (not shown), with a contribution to adiabatic cooling by

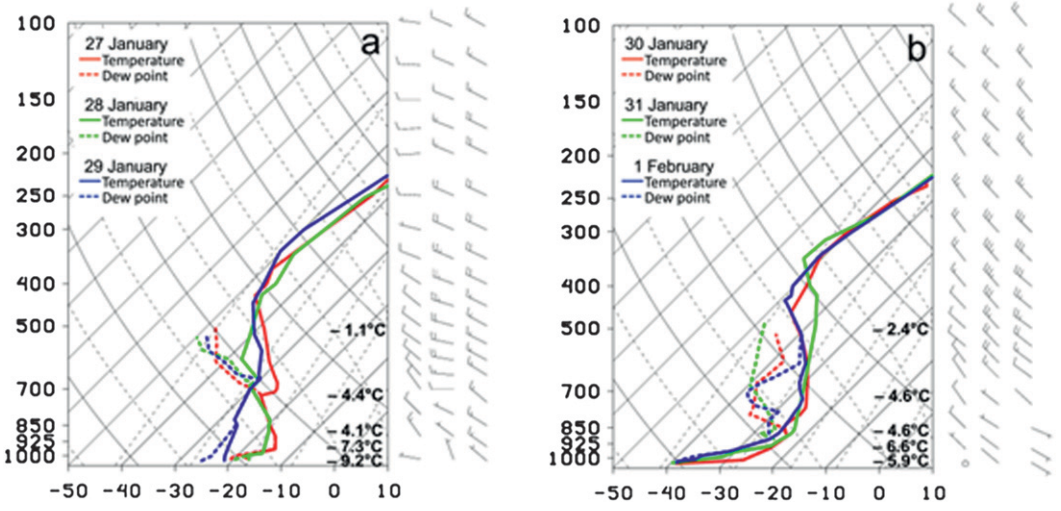

FIG. 4. (a),(b) Daily soundings at 1200 UTC 27 Jan–1 Feb 1979 at Norman Wells. Upper-level winds are plotted to the right of each panel in chronological order from left to right. The 3-day change in temperature (°C) at 1000, 925, 850, 700, and 500 hPa is also shown in boldface on the right-hand side of each panel.

TABLE 3. Formation period daily (1200–1200 UTC) thermodynamic budget terms (°C day^{-1} ± the standard error), from interpolated to the northern (Sachs Harbour, Inuvik, Kuluktuk, Norman Wells, and Yellowknife) and southern stations (Fort Simpson, Fort Smith, Fort Nelson, Fort McMurray, and Grande Prairie) and averaged over lower (1000–850 hPa) and upper levels (850–500 hPa). Cooling greater than 1°C day^{-1} are in boldface.

	Northern stations							
	1000–850 hPa				850–500 hPa			
	Temperature change	Horizontal advection	Vertical term	Residual	Temperature change	Horizontal advection	Vertical term	Residual
27–28 Jan	**−2.8 ± 1.3**	−0.6 ± 1.5	−0.6 ± 1.0	**−1.6 ± 0.9**	**−4.4 ± 1.3**	**−2.1 ± 1.1**	0.3 ± 0.9	**−2.0 ± 0.7**
28–29 Jan	**−4.0 ± 1.2**	**−2.5 ± 1.6**	0.1 ± 0.5	**−1.6 ± 0.8**	**−1.3 ± 1.0**	0.2 ± 1.0	0.5 ± 0.3	**−2.0 ± 0.2**
29–30 Jan	**−2.1 ± 1.7**	−0.6 ± 2.0	2.3 ± 1.2	**−3.8 ± 1.6**	**−1.0 ± 1.0**	−0.1 ± 1.3	2.0 ± 0.5	**−2.9 ± 0.6**
30–31 Jan	**−1.8 ± 0.9**	−0.1 ± 1.0	2.2 ± 0.9	**−3.9 ± 1.2**	**−1.2 ± 0.7**	0.2 ± 1.0	1.6 ± 0.8	**−3.0 ± 0.8**
31 Jan–1 Feb	**−2.0 ± 1.0**	−0.5 ± 0.7	0.1 ± 0.9	**−1.7 ± 0.7**	**−1.6 ± 0.8**	0.2 ± 0.7	0.0 ± 0.5	**−1.5 ± 0.8**
1–2 Feb	**−1.7 ± 1.2**	0.5 ± 1.1	−1.3 ± 1.6	−0.9 ± 1.0	0.0 ± 1.0	1.1 ± 1.1	−0.4 ± 1.7	**−1.3 ± 0.7**
	Southern stations							
27–28 Jan	**−2.7 ± 1.6**	−0.2 ± 1.0	1.2 ± 1.0	**−3.7 ± 1.0**	**−4.6 ± 2.2**	**−5.5 ± 2.2**	2.8 ± 0.9	**−1.8 ± 0.4**
28–29 Jan	**−1.7 ± 1.3**	1.8 ± 1.5	0.8 ± 0.6	**−4.2 ± 1.1**	0.3 ± 1.6	1.6 ± 1.2	1.1 ± 1.0	**−2.4 ± 0.5**
29–30 Jan	**−5.5 ± 1.0**	**−3.0 ± 1.4**	−0.5 ± 1.2	**−2.0 ± 0.6**	**−3.7 ± 1.2**	**−1.5 ± 1.2**	−0.9 ± 1.4	**−1.3 ± 0.6**
30–31 Jan	**−3.2 ± 1.7**	**−2.2 ± 1.2**	0.0 ± 1.1	**−1.0 ± 0.8**	**−1.8 ± 2.0**	**−1.2 ± 0.9**	−0.4 ± 1.8	−0.3 ± 0.6
31 Jan–1 Feb	**−1.0 ± 1.1**	−0.1 ± 0.7	−0.3 ± 0.7	−0.7 ± 0.8	−0.9 ± 1.1	−0.4 ± 0.9	−0.3 ± 1.0	−0.3 ± 0.5
1–2 Feb	0.2 ± 1.3	0.3 ± 1.1	−0.2 ± 0.9	0.1 ± 0.8	1.3 ± 1.2	3.1 ± 1.7	**−1.2 ± 1.4**	−0.7 ± 0.7

ascent on those days. The diabatic term was consistently negative—unlike advection, which was both warm and cold over the formation period. The residual was also the greatest contributor to the cooling at the northern and southern stations, indicating that the air mass intensified in situ, rather than being advected from another region.

There were multiple ways that radiative processes contributed to the diabatic cooling during the formation. These include radiation from cloud tops (Fig. 4a) when snow was reported at the surface on 27–29 January (Table 2). This process can be a mechanism for cloud growth; as the cloud top cools, condensation forms there, increasing the height of the cloud (Curry 1983; Emanuel 2008). As the formation continued, 29–31 January, the anticyclone in northwestern Canada intensified from 1024 to 1032 hPa (Figs. 3d,e), while its associated adiabatic warming increased (Table 3), drying and clearing the atmosphere. The surface temperature fell rapidly over this period (Table 2) aided by radiative cooling from fresh snow cover. Fresh snow has high emissivity, measured to be 0.98 in the atmospheric infrared window between 8 and 14 μm by Shafer and Super (1971), where as old snow has a lower emissivity of approximately 0.65 (Hewison and English 1999). After saturation with respect to ice was reached, ice fog formed (Table 2) under a temperature inversion (Fig. 4). The ice fog prevents further surface cooling but the top of a fog layer will cool radiatively and deepen by the same mechanism as cloud tops, lifting the height of the temperature inversion (Curry 1983). Also, ice crystals in the upper atmosphere cool the layer in which they are embedded.

4. Maintenance

a. Synoptic overview

During the maintenance period, 2–13 February, surface temperatures remain relatively constant compared to the formation period. Norman Wells, a station centrally located in the air mass, remains within 6°C of the mean value, −43.0°C (Fig. 2a). The arctic air mass, as measured by thickness anomaly, underwent cycles of intensification and weakening. Figure 5 shows daily minimum surface temperature and the 1000–500-hPa thickness anomalies at Norman Wells in Fig. 2, along with the mean surface dewpoint temperature, for the maintenance period. Periods of intensification, as defined by decreasing thicknesses, are 5–6, 6–7, 9–10, and 11–12 February. Periods of weakening are 4–5, 7–8, 8–9, and 10–11 February.

Deep-layer cooling is not always coincident with surface temperature falls. For example, on 6–7 February, the surface temperature rose while the thicknesses anomalies fell to their coldest. On the following day, 7–8 February, the surface temperature fell while the thicknesses warmed. Surface cooling occurs when clear skies are reported while thicknesses fall in the presence of ice crystals.

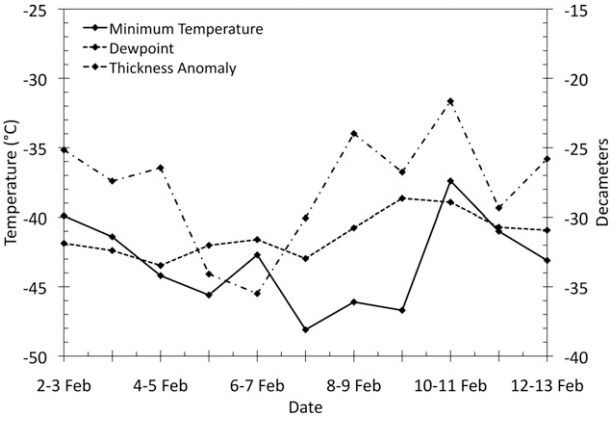

FIG. 5. Daily (1200–1200 UTC) minimum surface temperature (solid, °C), mean surface dewpoint temperature (dotted–dashed, °C), and mean 1000–500-hPa thickness anomalies (dashed, dam) at Norman Wells for each day in the maintenance period.

Figure 6 shows the sea level pressure, 700-hPa winds and 1000–500-hPa thickness at 1200 UTC daily during the maintenance period. On the first day, 2 February (Fig. 6a), the Aleutian low was still to the west of its climatological position in the Gulf of Alaska, as during the formation period. Consequently, the Pacific–North American (PNA) teleconnection (Wallace and Gutzler 1981) was in an extremely negative phase, with a value of −1.7. A negative phase PNA is associated with anticyclone formation and blocking in northwestern Canada (Croci-Maspoli et al. 2007).

By 4 February (Fig. 6c), the 1000–500-hPa thickness contours show an upper-level trough present over the Aleutian Islands, indicating cyclonic vorticity in that region, while cold 1000–500-hPa thickness anomalies drained through the Alaskan highlands and lowlands into the Gulf of Alaska. At the edge of the outflowing arctic air, a cyclone formed and deepened from 1002 hPa from 0000 UTC 4 February to 980 hPa at 0000 UTC 5 February in association with cyclonic vorticity advection from the upper-level trough (not shown). The cyclone was subsequently driven over the Rocky Mountains to the south of the cold air mass, transporting moisture (not shown) into the interior.

Throughout the maintenance period, the coldest thicknesses are located over their climatological position in the Canadian archipelago, but build westward into northwestern Canada, centered on Great Bear Lake (to the east of Norman Wells, Fig. 1), on 6–7 (Figs. 6e,f) and 12–13 February (Figs. 6j,k). A high–low pressure couplet, with higher pressure and a cold pool in the lee of the mountains, warmer air and low pressure over the Gulf of Alaska and a pressure and temperature gradient parallel to the mountains was created by the end of the formation period (Fig. 3f). The anticyclone east of the mountains was very strong, with sea level pressure above 1040 hPa on 3 February (Fig. 6b). It weakened slightly from 4–6 February but intensified above 1040 hPa again from 7–10 February and again on 12 February. Cyclonic circulations broke off from the Aleutian low on 5, 7, and 9 February (Figs. 6g,i,k), whose tracks were deflected to the south of the cold pool, along the pressure gradient, from northwest to southeast. The cold pool and anticyclone block onshore movement of cyclones, with associated cloudiness and precipitation into the region, keeping the air mass in place.

This structure (Figs. 5–6) is an example of cold-air damming. Cold-air damming in a climatological sense has been identified in several locations in the United States, most notably in the Appalachian Mountains along the North American east coast (Bell and Bosart 1988). To the east of the Appalachians and other midlatitude mountain chains, a shallow dome of cold air and high pressure can form, blocking surface cyclone movement into the region. The mechanisms responsible have been found to be adiabatic expansion and cooling from anabatic flow (Forbes et al. 1987) causing cloud formation, precipitation, and subsequent evaporative cooling below (Fritsch et al. 1992). Although to our knowledge it is only rarely mentioned in the literature (Turner and Gyakum 2011; Szeto 2008), cold-air damming is common on the lee side of Alaskan and Mackenzie Ranges and is a crucial element of arctic airmass formation in the region. The damming isolates the cold pool, preventing it from mixing with warmer air and allowing the cumulative effect of incremental radiational cooling to become large.

The sea level pressure and 1000–500-hPa thickness anomalies at 1200 UTC each day of the maintenance period are shown in Figs. 7a–l. Throughout the maintenance period, high pressure anomalies of 24 hPa or greater were present in northwestern Canada from 7–12 February (Figs. 7f–k). There were weaker low pressure anomalies in the Gulf of Alaska and the periodic lows that entered the continental interior can be seen in the anomalies fields on 5, 7, and 9 February (Figs. 7d,f,h).

The cold pool, as seen in the 1000–500-hPa anomalies (Fig. 5), underwent cycles of intensification and weakening. At the start of the maintenance period, 2–3 February (Figs. 6a,b), the coldest thickness anomalies were elongated, stretching from northwest to southeast to the east of the mountains, with the coldest anomaly located over northern Alberta. The cold pool intensified and on 4 February (Fig. 7c) the coldest 1000–500-hPa anomalies, −32 dam, were centered between Great Slave and Great Bear Lakes. Cold air began to drain through the Alaskan lowlands into the Gulf of Alaska.

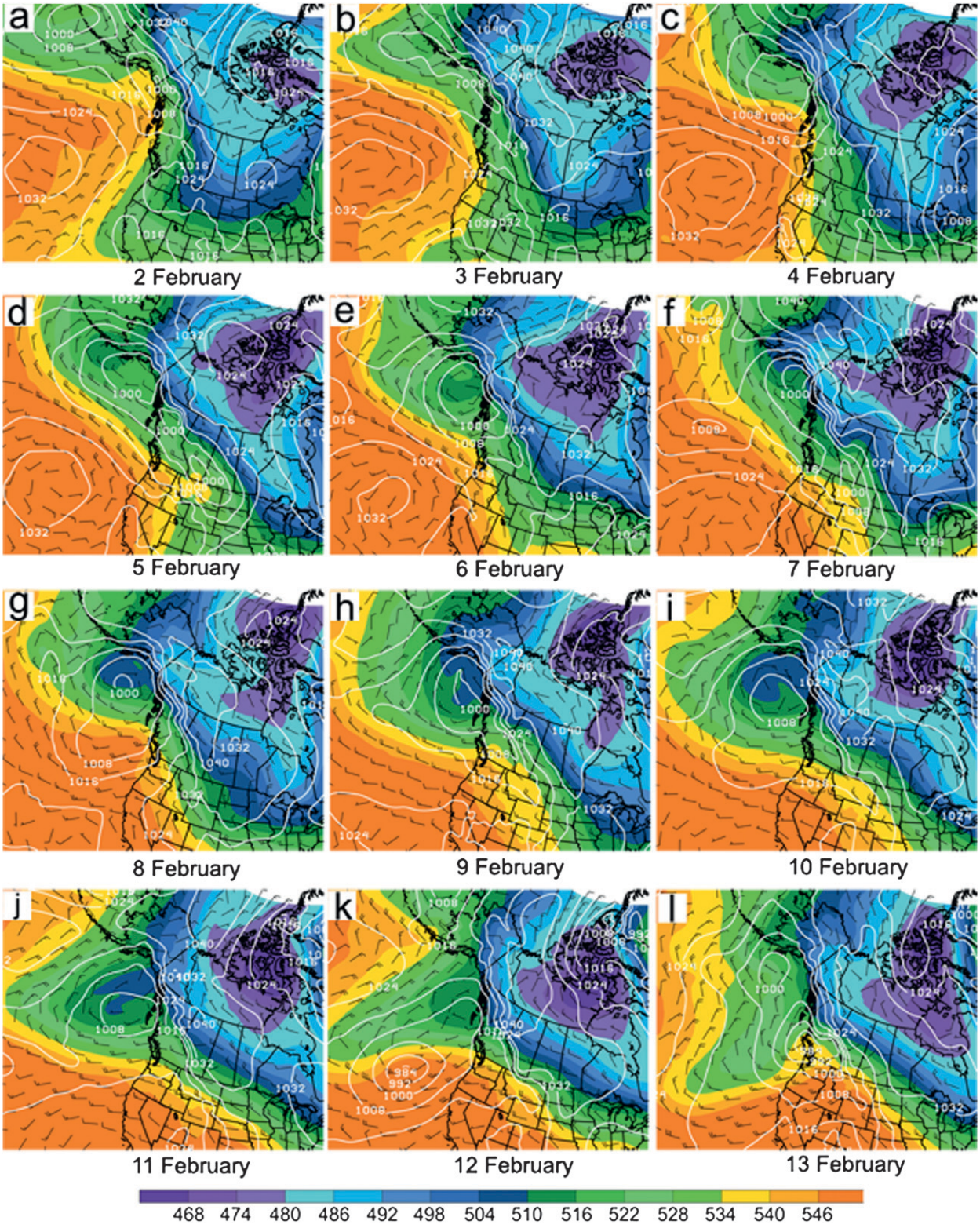

FIG. 6. Sea level pressure (contours, hPa), 700-hPa winds (barbs, m s^{-1}), and 1000–500-hPa thicknesses (shaded, dam) at 1200 UTC daily during the maintenance period.

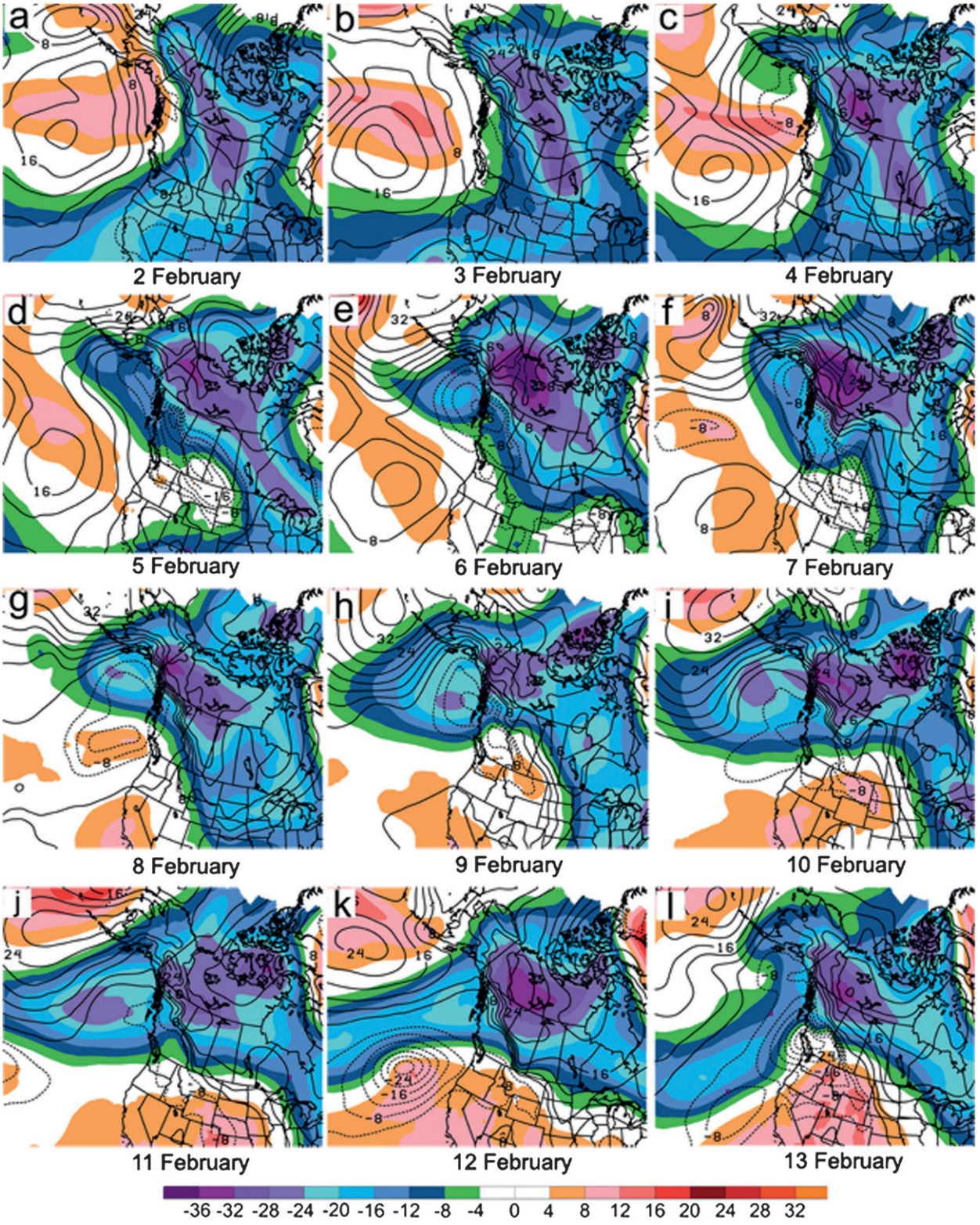

FIG. 7. Sea level pressure anomalies (contours, hPa, dashed for negative anomalies) and 1000–500-hPa thickness anomalies (shaded, dam) at 1200 UTC daily during the maintenance period.

TABLE 4. Mean surface temperature and weather reports (as a percentage of total reports) at the northern stations (Sachs Harbour, Inuvik, Kugluktuk, Norman Wells, and Yellowknife) and southern stations (Fort Simpson, Fort Smith, Fort Nelson, Fort McMurray, and Grande Prairie) from 1200–1200 UTC on each day of the maintenance period. Most frequent observations on a given day are in boldface.

	Surface temperature (°C)	Clear/mainly clear	Cloudy/mostly cloudy	Ice crystals/ice fog	Snow/blowing snow
			Northern stations		
2–3 Feb	−36.3	22	6	**67**	5
3–4 Feb	−37.0	28	0	**58**	15
4–5 Feb	−38.8	35	8	**56**	1
5–6 Feb	−37.9	17	9	**60**	14
6–7 Feb	−39.8	14	8	**71**	8
7–8 Feb	−39.7	**51**	3	36	10
8–9 Feb	−39.6	35	7	**47**	12
9–10 Feb	−38.5	13	7	**71**	9
10–11 Feb	−36.4	**40**	6	36	18
11–12 Feb	−36.7	29	12	**55**	3
12–13 Feb	−35.3	**60**	6	32	2
			Southern stations		
2–3 Feb	−30.4	28	6	16	**50**
3–4 Feb	−29.3	7	18	28	**47**
4–5 Feb	−31.5	31	6	13	**50**
5–6 Feb	−31.5	13	21	21	**45**
6–7 Feb	−30.0	11	9	19	**61**
7–8 Feb	−31.2	12	8	21	**60**
8–9 Feb	−34.4	30	27	10	**33**
9–10 Feb	−30.9	7	7	24	**62**
10–11 Feb	−32.9	**36**	9	24	32
11–12 Feb	−30.5	28	31	8	**33**
12–13 Feb	−32.2	38	8	7	**48**

On 6–7 February (Figs. 7e,f), the cold pool was at its most intense, with thickness anomalies below −48 dam. There was pressure-driven gap outflow through the coastal mountains at this time, particularly around Juneau, Alaska. From 8–9 February (Figs. 7g,h), the cold pool weakened, continuing to drain into the gulf through gap flow. There was a slight intensification, shown by decreased thicknesses in the Yukon on 10 February (Fig. 7i), another weakening on 11 February (Fig. 6j), and a final reintensification on 12 February (Fig. 7k).

Weather reports during the maintenance period, presented in Table 4, indicate near saturation at the surface. The most frequent weather reported at the northern stations was ice crystals and ice fog, except on 7–8, 10–11, and 12–13 February, when clear skies were reported. On those dates when clear skies were reported, thicknesses at Norman Wells increased (Fig. 5). The deep-layer cold pool is weakest on 8 and 11 February (Figs. 6g,j) at the end of the clear-sky periods. By contrast, the southern stations, located on the edge of the cold pool, received almost continuous snow as the succession of cyclones (Figs. 6d,f,h), impacted the area, with the exception of 10–11 February when clear skies were reported simultaneously with the northern stations. The thermodynamic consequences of these weather reports will be discussed in the following section.

b. The thermodynamic budget

The thermodynamic budget of the 1000–850- and 850–500-hPa layers at the northern and southern stations is given in Table 5. At both the northern and southern stations the magnitude of daily temperature changes is smaller than in the formation period—the average absolute value of temperature change is 1.4°C during the maintenance period, but 2.4°C during formation—and oscillates between warming and cooling. At the northern stations, the absolute value of the magnitude of horizontal advection is the smallest of all the terms, but since the advection is mostly warm advection in both the lower and upper layers, it is responsible for significant cumulative warming. There was adiabatic cooling in the upper and lower layers from 2–6 February when the 700-hPa winds (Figs. 6a–e) at the northern stations had upslope easterlies toward the low in the gulf. For the remainder of the maintenance period, adiabatic warming occurred, producing warming comparable to the advective term. The residual was generally larger in the 850–500-hPa layer and contributed to cooling on most days. On average, this term balanced the net warming from the advective and vertical terms. A notable exception is from the 7–8 February, when the residual in the 850–500-hPa layer was nearly zero, in the absence of radiation cooling

TABLE 5. Maintenance period daily thermodynamic budget terms (°C day^{-1} ± the standard error), from 1200–1200 UTC interpolated to the northern (Sachs Harbour, Inuvik, Kuluktuk, Norman Wells, and Yellowknife) and southern stations (Fort Simpson, Fort Smith, Fort Nelson, Fort McMurray, and Grande Prairie) and averaged over lower (1000–925 hPa) and upper levels (850–500 hPa). Cooling greater than 1°C day^{-1} are in boldface.

	Northern stations							
	1000–850 hPa				850–500 hPa			
	Temperature change	Horizontal advection	Vertical term	Residual	Temperature change	Horizontal advection	Vertical term	Residual
2–3 Feb	**−2.2 ± 1.0**	1.2 ± 1.8	**−2.8 ± 1.4**	−0.7 ± 0.6	−0.8 ± 1.0	1.3 ± 1.0	**−1.7 ± 0.8**	−0.4 ± 0.5
3–4 Feb	1.3 ± 1.4	1.3 ± 1.6	−0.1 ± 0.9	0.1 ± 0.8	−0.2 ± 1.1	1.3 ± 1.2	0.1 ± 1.1	**−1.5 ± 0.9**
4–5 Feb	**−1.3 ± 1.**7	0.2 ± 1.3	−0.6 ± 0.8	−0.9 ± 1.1	−0.8 ± 1.6	0.5 ± 1.1	0.3 ± 1.1	**−1.8 ± 0.8**
5–6 Feb	−0.6 ± 0.5	0.3 ± 0.6	0.3 ± 0.8	**−1.1 ± 1.1**	**−1.3 ± 0.5**	0.7 ± 0.7	**−1.3 ± 0.8**	−0.9 ± 0.7
6–7 Feb	−0.5 ± 1.1	0.0 ± 1.1	−0.1 ± 1.1	−0.5 ± 1.1	2.4 ± 1.2	1.9 ± 1.2	1.6 ± 1.3	−0.2 ± 1.1
7–8 Feb	2.8 ± 1.5	0.8 ± 1.5	1.2 ± 2.1	0.7 ± 1.5	1.8 ± 1.8	1.2 ± 1.1	1.3 ± 1.6	**−1.0 ± 1.0**
8–9 Feb	**−1.6 ± 1.1**	0.5 ± 1.8	1.0 ± 1.2	**−2.9 ± 1.4**	−0.2 ± 1.3	0.1 ± 0.9	1.9 ± 0.9	**−2.8 ± 0.8**
9–10 Feb	1.6 ± 1.3	1.5 ± 1.8	1.3 ± 0.9	**−1.3 ± 1.0**	**−1.0 ± 1.4**	1.0 ± 1.5	0.7 ± 1.1	**−2.1 ± 0.5**
10–11 Feb	−0.5 ± 1.3	0.2 ± 1.2	1.5 ± 1.2	**−2.1 ± 0.9**	−0.7 ± 1.1	0.0 ± 1.3	0.5 ± 0.9	**−2.1 ± 0.9**
11–12 Feb	1.0 ± 1.6	1.4 ± 2.1	−0.7 ± 1.2	0.2 ± 1.1	**−1.4 ± 1.4**	−0.6 ± 2.0	1.2 ± 1.3	−1.3 ± 0.9
12–13 Feb	2.6 ± 1.3	**−1.2 ± 3.2**	4.2 ± 1.7	−0.6 ± 2.8	1.9 ± 0.8	0.4 ± 2.1	3.7 ± 1.5	**−2.2 ± 0.7**
	Southern stations							
2–3 Feb	**−2.7 ± 0.7**	**−2.1 ± 1.7**	0.3 ± 0.6	−0.9 ± 1.4	1.2 ± 1.3	3.1 ± 1.7	**−1.2 ± 2.7**	−0.6 ± 1.4
3–4 Feb	−0.5 ± 0.9	**−1.1 ± 1.6**	0.5 ± 0.6	0.0 ± 1.4	−0.5 ± 1.2	2.8 ± 2.0	**−1.6 ± 1.2**	**−1.7 ± 1.1**
4–5 Feb	**−1.1 ± 1.0**	−0.8 ± 2.9	**−3.4 ± 2.4**	3.1 ± 2.4	1.2 ± 1.4	5.3 ± 2.3	**−7.1 ± 4.5**	3.0 ± 2.7
5–6 Feb	0.7 ± 1.3	−0.8 ± 2.1	−0.8 ± 1.0	2.3 ± 1.8	−0.9 ± 1.6	1.8 ± 1.8	**−1.4 ± 1.6**	**−1.3 ± 1.6**
6–7 Feb	**−1.9 ± 2.8**	−0.5 ± 4.3	**−4.5 ± 3.5**	3.1 ± 3.9	−0.2 ± 2.8	6.7 ± 2.5	**−8.5 ± 4.4**	1.6 ± 3.7
7–8 Feb	**−2.1 ± 1.8**	**−1.4 ± 1.3**	**−1.9 ± 1.0**	1.2 ± 1.4	**-2.3 ± 2.3**	0.3 ± 1.2	1.4 ± 1.5	**−1.1 ± 1.4**
8–9 Feb	1.7 ± 1.2	1.2 ± 2.0	**−2.2 ± 2.2**	2.7 ± 1.8	4.9 ± 1.5	6.7 ± 1.7	**−3.4 ± 3.3**	1.5 ± 2.3
9–10 Feb	−0.6 ± 1.0	**−1.5 ± 1.3**	**−1.8 ± 1.4**	2.7 ± 1.1	**−4.7 ± 1.6**	**−2.0 ± 2.0**	**−3.3 ± 2.8**	0.6 ± 1.8
10–11 Feb	0.8 ± 1.7	**−1.0 ± 1.4**	−0.1 ± 1.7	−0.2 ± 0.8	0.9 ± 1.4	0.4 ± 1.9	1.5 ± 1.9	**−1.0 ± 0.8**
11–12 Feb	−0.8 ± 1.5	−0.2 ± 1.6	0.9 ± 1.9	**−1.4 ± 1.4**	**−1.4 ± 1.8**	0.5 ± 3.0	0.0 ± 2.6	**−1.8 ± 1.3**
12–13 Feb	**−1.3 ± 1.0**	0.7 ± 1.8	**−2.3 ± 2.8**	0.3 ± 2.0	−0.1 ± 2.0	5.1 ± 3.2	**−4.3 ± 4.0**	−0.9 ± 2.2

from ice crystals. At this time, clear skies were reported (Table 4) and the cold pool weakened (Fig. 5).

At the southern stations, the terms are generally larger than at the northern stations, especially the vertical term. There are differences in the sign of horizontal advection between the upper and lower layers, as warm advection from Pacific cyclones occurs above the colder surface air. Three major periods of upper-level warm air advection is 4–5, 6–7, and 8–9 February, as low pressure centers broke off from the main circulation in the gulf and passed into the interior. Low pressure was present over the western United States on 5, 7, and 9 February (Figs. 6d,f,h). The ascent contributes to cooling (Table 5) in the presence of snow (Table 4). The residual is positive in the lower levels, consistent with reports of snow (Table 3), suggesting downwelling radiation from cloud cover. The residual term alternates between warming and cooling in the 850–500-hPa layer, likely controlled by cloud thickness and height with their associated latent heating and cloud-top cooling. In the net for the lower layer, cold-air advection can entirely account for the modest amount of cooling in this layer, while the diabatic processes produce significant warming that compensates for the significant cooling from the upward motion. For the upper layer, the large cooling by the vertical motion is compensated for by the warming from horizontal advection, with the diabatic term contributing very little to the net temperature change.

Figure 8 shows soundings at Norman Wells and Fort Nelson at 1200 UTC 6 February, as a low pressure pulse is beginning to cross the mountains (Fig. 6e) and the air mass begins its strongest intensification (Fig. 5). At Norman Wells, there were no winds from 1000–925 hPa. A weak surface inversion existed, but the entire troposphere was colder than −30°C, with high levels of saturation. The tropopause was extremely low at approximately 500 hPa. The Fort Nelson sounding was associated with two separate air masses. The arctic air cold pool was banked up to the level of the mountains, characterized by much colder air and southeasterly winds. Aloft, the air was warmer, conditionally unstable and saturated, with winds from the west, as the Pacific air overran the arctic air.

Periods of airmass weakening are characterized by an absence of moisture. For example, on 7–8 February

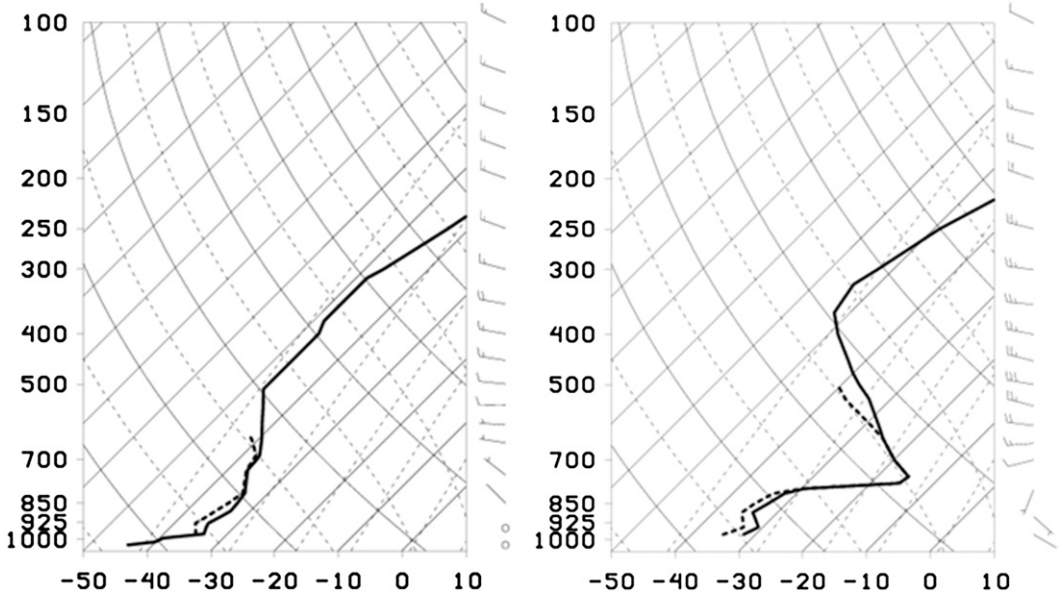

FIG. 8. Soundings at 1200 UTC 6 Feb 1979 at (left) Norman Wells and (right) Fort Nelson.

clear skies, rather than ice crystals, are the most frequent weather report at the northern stations (Table 4) during which time the cold-pool thickness anomaly (Fig. 5) weakens. The thermodynamic budget (Table 5) shows the temperature in the 1000–850-hPa layer increases by 2.8°C on this day, largely owing to adiabatic warming and the absence of residual cooling over that period, though advective warming was also significant.

5. Dissipation

A fast-moving Pacific cyclone approaches North America from the southwest on 12 February and comes onshore of Washington State on 13 February (Figs. 6j,k). Figure 9 is the sea level pressure, 700-hPa winds, and 1000–500-hPa thickness at 1200 UTC for three days following the event. On 14 February, the cyclone is in the U.S. Intermountain West (Fig. 9a). At this time, the flow is zonal over the United States and southern Canada but after the passage of the cyclone from 15–16 February (Figs. 9b,c), the steering flow over the arctic air mass has a meridional component. The 300-hPa steering flow has been altered by the passage of the low (not shown) and is now northwesterly across western North America, with ridging present over the Rocky Mountains.

The cold pool and its associated 1040-hPa anticyclone move quickly to the southeast across the Midwest of the United States in the northwesterly flow on 16 February.

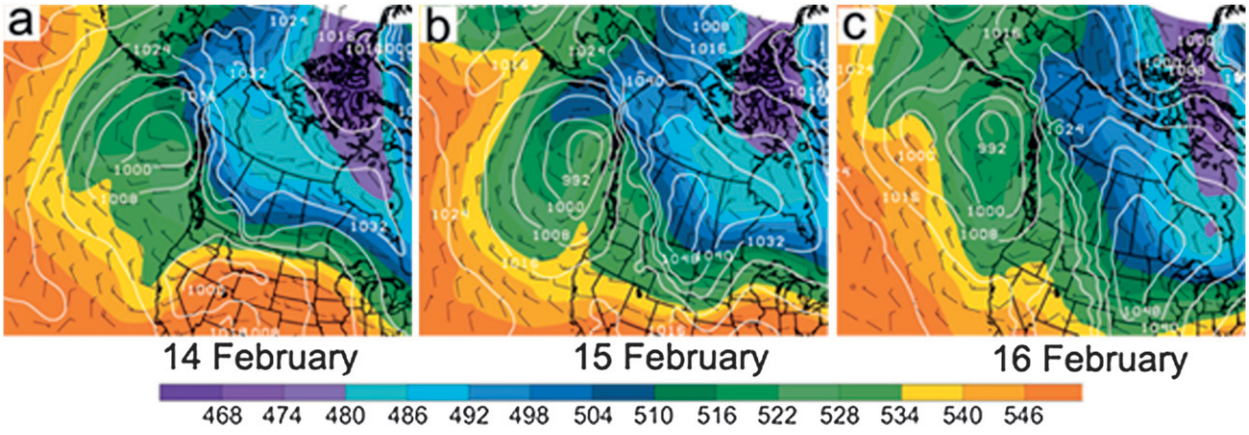

FIG. 9. Sea level pressure (contours, hPa), 700-hPa winds (barbs, m s^{-1}), and 1000–500-hPa thicknesses (shaded, dam) at 1200 UTC daily during the dissipation period.

This air mass goes on to act as a precursor for the well-studied (Bosart 1981; Bosart and Lin 1984; Spaete et al. 1994; Uccellini et al. 1985, 1984) explosive cyclogenesis, the Presidents' Day storm of 1979 when it traveled toward the mid-Atlantic coast.

6. Summary and conclusions

Arctic air masses in northwestern Canada have been shown to be climatologically deep-layer phenomena, with a multistage formation process in the presence of moisture (Turner and Gyakum 2011), contrary to the original formulation of shallow, dry, surface-cooling-driven events. This paper has described a specific event in February 1979 that, while displaying typical formation behavior, was notable for its intensity and longevity. It also underwent several cycles of weakening and intensification, allowing for a close investigation of physical mechanisms and quantification of their relative contributions.

The formation began with snow falling in northwestern Canada (Table 2). Soundings showed (Fig. 4) that the 1000–700-hPa layer began to cool before the surface, through diabatic processes (Table 3) until the atmospheric profile was stable. After the snow abated, rapid radiative cooling took place at the surface (Fig. 4). When the surface cooled below its frost point, ice crystals formed and ice fog was reported (Table 2). Ice fog dampens radiative cooling from the surface but radiative cooling at the top of the layer is enhanced, acting to raise the height of surface temperature inversions. Once the air mass developed, it created a cold-air damming circulation in the lee of the Pacific Rockies (Figs. 6 and 7) with a high–low pressure couplet and a baroclinic zone, characterized by intense gradients of temperature and pressure, parallel to the mountains. The formation was shown to be caused primarily by diabatic processes, including radiative and possibly sublimation effects, as the lower troposphere becomes saturated.

During the maintenance of the event, periods of airmass intensification and decreased thicknesses were characterized by high (greater than 100%) values of relative humidity with respect to ice (not shown), reports of ice crystals or ice fog at the northern stations (Table 4) and diabatic cooling (Table 5). However, the surface temperature did not change temperature significantly (Table 4), consistent with ice crystal radiative processes. Periods of airmass weakening corresponded to a majority of weather reports (Table 4) of clear skies.

A Gulf of Alaska cyclone was present throughout the maintenance period with periodic intrusions of low pressure over the Rocky Mountains, along the baroclinic zone, from the main system and into the continental interior. At these times, there was moisture transport (not shown) aloft into northwestern Canada and subsequent precipitation of snow or ice crystals and sublimation in the lower levels, replenishing moisture there. This process maintained the humidity of the air mass, allowing for further radiative cooling, acting against subsidence warming, and maintaining the structure of the air mass.

The importance of moisture in different phases to the formation, intensification, and maintenance of a historical air mass has been suggested in this investigation, confirming the results from modeling studies (Curry 1983; Emanuel 2008). This airmass life cycle was also shown to be associated with deep-layer, cold-air damming, contrary to the classical conception of shallow, surface-cooled air masses. The importance of diabatic cooling to arctic airmass formation suggests that the associated processes may be a particular challenge for both medium-range forecast and climate models. Though we have not addressed this issue here, the topic is appropriate to address in future work.

Acknowledgments. This research has been supported by a Natural Sciences and Engineering Research Council of Canada Discovery Grant and an International Polar Year Program Grant. We thank Lucie Vincent of Environment Canada for providing the corrected daily temperature dataset. We would also like to thank Professor Kerry Emanuel and two anonymous reviewers for their helpful comments on an earlier version of this manuscript.

REFERENCES

Bell, G. D., and L. F. Bosart, 1988: Appalachian cold-air damming. *Mon. Wea. Rev.,* **116,** 137–161.

Bosart, L. F., 1981: The Presidents' Day Snowstorm of 18–19 February 1979: A subsynoptic-scale event. *Mon. Wea. Rev.,* **109,** 1542–1566.

——, and S. C. Lin, 1984: A diagnostic analysis of the Presidents' Day Storm of February 1979. *Mon. Wea. Rev.,* **112,** 2148–2177.

Croci-Maspoli, M., C. Schwierz, and H. Davies, 2007: Atmospheric blocking: Space-time links to the NAO and PNA. *Climate Dyn.,* **29,** 713–725.

Curry, J., 1983: On the formation of continental polar air. *J. Atmos. Sci.,* **40,** 2278–2292.

Emanuel, K., 2008: Back to Norway: An essay. *Synoptic–Dynamic Meteorology and Weather Analysis and Forecasting, Meteor. Monogr.,* No. 33, Amer. Meteor. Soc., 87–96.

Forbes, G. S., R. A. Anthes, and D. W. Thomson, 1987: Synoptic and mesoscale aspects of an Appalachian ice storm associated with cold-air damming. *Mon. Wea. Rev.,* **115,** 564–591.

Fritsch, J. M., J. Kapolka, and P. A. Hirschberg, 1992: The effects of subcloud-layer diabatic processes on cold air damming. *J. Atmos. Sci.,* **49,** 49–70.

Girard, E., and J.-P. Blanchet, 2001: Simulation of Arctic diamond dust, ice fog, and thin stratus using an explicit aerosol–cloud–radiation model. *J. Atmos. Sci.,* **58,** 1199–1221.

Gotaas, Y., and C. S. Benson, 1965: The effect of suspended ice crystals on radiative cooling. *J. Appl. Meteor.,* **4,** 446–453.

Hewison, T. J., and S. J. English, 1999: Airborne retrievals of snow and ice surface emissivity at millimeter wavelengths. *IEEE Trans. Geosci. Remote Sens.,* **37,** 1871–1879.

Intrieri, J. M., and M. D. Shupe, 2004: Characteristics and radiative effects of diamond dust over the western Arctic Ocean region. *J. Climate,* **17,** 2953–2960.

——, C. W. Fairall, M. D. Shupe, P. O. G. Persson, E. L Andreas, P. S. Guest, and R. E. Moritz, 2002: An annual cycle of Arctic surface cloud forcing at SHEBA. *J. Geophys. Res.,* **107,** 8039, doi:10.1029/2000JC000439.

Jones, P. D., and A. Moberg, 2003: Hemispheric and large-scale surface air temperature variations: An extensive revision and an update to 2001. *J. Climate,* **16,** 206–223.

Lackmann, G. M., J. R. Gyakum, and R. Benoit, 1998: Moisture transport diagnosis of a wintertime precipitation event in the Mackenzie River basin. *Mon. Wea. Rev.,* **126,** 668–692.

Liu, J., J. A. Curry, W. B. Rossow, J. R. Key, and X. Wang, 2005: Comparison of surface radiative flux data sets over the Arctic Ocean. *J. Geophys. Res.,* **110,** C02015, doi:10.1029/2004JC002381.

Mesinger, F., and Coauthors, 2006: North American Regional Reanalysis. *Bull. Amer. Meteor. Soc.,* **87,** 343–360.

Rogers, R. R., and M. K. Yau, 1989: *A Short Course in Cloud Physics.* Butterworth-Heinemann, 290 pp.

Serreze, M. C., and J. Francis, 2006: The Arctic amplification debate. *Climatic Change,* **76,** 241–264.

——, and Coauthors, 2000: Observational evidence of recent change in the northern high-latitude environment. *Climatic Change,* **46,** 159–207.

Shabbar, A., and B. Bonsal, 2003: An assessment of changes in winter cold and warm spells over Canada. *Nat. Hazards,* **29,** 173–188, doi:10.1023/A:1023639209987.

Shafer, B. A., and A. B. Super, 1971: Infrared temperature sensing of snow covered terrain. Final Report under Contract DAHC04-67-C0058, Montana State University, 99 pp.

Sorteberg, A., V. Kattsov, J. Walsh, and T. Pavlova, 2007: The Arctic surface energy budget as simulated with the IPCC AR4 AOGCMs. *Climate Dyn.,* **29,** 131–156.

Spaete, P., D. R. Johnson, and T. K. Schaack, 1994: Stratospheric–tropospheric mass exchange during the Presidents' Day Storm. *Mon. Wea. Rev.,* **122,** 424–439.

Szeto, K. K., 2008: On the extreme variability and change of cold-season temperatures in northwest Canada. *J. Climate,* **21,** 94–113.

Town, M. S., V. P. Walden, and S. G. Warren, 2005: Spectral and broadband longwave downwelling radiative fluxes, cloud radiative forcing, and fractional cloud cover over the South Pole. *J. Climate,* **18,** 4235–4252.

Turner, J. K., and J. R. Gyakum, 2011: The development of Arctic air masses in Northwest Canada and their behavior in a warming climate. *J. Climate,* **24,** 4618–4633.

Uccellini, L. W., P. J. Kocin, R. A. Petersen, C. H. Wash, and K. F. Brill, 1984: The Presidents' Day cyclone of 18–19 February 1979: Synoptic overview and analysis of the subtropical jet streak influencing the pre-cyclogenetic period. *Mon. Wea. Rev.,* **112,** 31–55.

——, D. Keyser, K. F. Brill, and C. H. Wash, 1985: The Presidents' Day cyclone of 18–19 February 1979: Influence of upstream trough amplification and associated tropopause folding on rapid cyclogenesis. *Mon. Wea. Rev.,* **113,** 962–988.

Vavrus, S., D. Waliser, A. Schweiger, and J. Francis, 2008: Simulations of 20th and 21st century Arctic cloud amount in the global climate models assessed in the IPCC AR4. *Climate Dyn.,* **33** (7–8), 1099–1115, doi:10.1007/s00382-008-0475-6.

Vincent, L. A., X. Zhang, B. R. Bonsal, and W. D. Hogg, 2002: Homogenization of daily temperatures over Canada. *J. Climate,* **15,** 1322–1334.

Wallace, J. M., and D. S. Gutzler, 1981: Teleconnections in the geopotential height field during the Northern Hemisphere winter. *Mon. Wea. Rev.,* **109,** 784–812.

Walsh, J. E., W. L. Chapman, and D. H. Portis, 2009: Arctic cloud fraction and radiative fluxes in atmospheric reanalyses. *J. Climate,* **22,** 2316–2334.

Wendler, G., 1969: Heat balance studies during an ice-fog period in Fairbanks, Alaska. *Mon. Wea. Rev.,* **97,** 512–552.

Wexler, H., 1936: Cooling in the lower atmosphere and the structure of polar continental air. *Mon. Wea. Rev.,* **64,** 122–136.

——, 1937: Formation of polar anticyclones. *Mon. Wea. Rev.,* **65,** 229–236.